High Performance Lamb Wave Resonator Operating in the 900 MHz ISM Band for Wireless Sensing Applications

Anne-Marie Zaccarin[*], Gokulanand M. Iyer[*], Abhay Kochhar[#], Ramakrishna Vetury[#], Kevin T. Turner[*], Roy H. Olsson III[*1]

[*]University of Pennsylvania, USA
[#]Akoustis Inc, USA
[1]rolsson@seas.upenn.edu

***Abstract* — Precision agriculture systems enabled by passive, wireless, subsurface soil sensors can provide high resolution data on soil conditions and increase crop yield. These frequency-coded sensor nodes are composed of an antenna, acoustic resonator and capacitive soil moisture sensor. Here, a high performance $Al_{0.7}Sc_{0.3}N$ Lamb-wave resonator (LWR) for operation in the 902-928 MHz industrial, scientific, medical (ISM) band is fabricated. Its figure of merit is 37% larger than state-of-the-art LWR at similar frequency. The LWR is integrated with a capacitive moisture sensor and its frequency tuning capabilities are demonstrated. A sensitivity of 65 kHz at interrogation ranges of up to 150 m is determined.**

***Keywords* — acoustic resonators, Lamb-wave resonators, Internet of Things.**

I. Introduction

Current agricultural practices rely on data from few, sparse soil samples gathered from different locations. Often, fields are too large to gain precise, local knowledge of soil properties. Precision agriculture systems enabled by internet of things (IoT) technologies, through high spatial resolution monitoring of field conditions, can facilitate more efficient deployment of agriculture resources and result in higher crop yield [1]. Inexpensive, passive, and mostly biodegradable sub-surface soil sensor nodes are essential to the deployment of such systems. The 902-928 MHz industrial, scientific, medical (ISM) band offers good penetration of radio-frequency (RF) signals in soil while still enabling relatively small antennas, making it ideal for this application [1].

Chip-based radio-frequency identification (RFID) methods for passive wireless sensing rely on the tuning of resonant antennas. Sensor node communication range is limited by the tank quality factor (Q). These antenna-chip sensor nodes are, essentially, parallel inductor-capacitor (LC) tanks [2]–[4]. They have Q factors on order of 100, and typical communication distances up to 10 m [5]. Their employment in the 902 MHz ISM band for frequency-coded tagging is further complicated by the limited ISM bandwidth. The sensor tag resonant frequency (f_0) would be pulled out of the band by a relatively small change in sensor capacitance.

Chipless RFID passive wireless sensor nodes with a theoretical interrogation distance of up to 40 m have been demonstrated [6]. These communication ranges are obtained at 2.4 GHz using RF cavities with a Q of 1000. These cavities, while ideal for building structural health monitoring, are prohibitively large ($\approx$ 706 cm^3) for precision agriculture.

Integrated acoustics offers a promising option for miniaturized high Q devices. Significant research has been reported on surface acoustic wave (SAW) passive sensor nodes [7]–[11]. These sensors use interdigitated transducers to launch a SAW into a delay line, before the SAW is reconverted into an electrical signal. Changes in measurand are calculated through changes in acoustic velocity (measured as a change in f_0 or time-of-flight) obtained from the delay line. The presence of this delay line inevitably introduces loss, limiting sensor communication range [9].

When using acoustic resonators to measure frequency shifts at long range, high figure of merit (FOM) ($Q_m \times k_t^2$) is critical. The maximal frequency shift of the system is directly proportional to the electromechanical coupling coefficient (k_t^2) of the resonator, while sensor sensitivity (or minimum detectable frequency shift Δf_{min}) improves with Q:

$$\Delta f_{min} = \frac{3\sqrt{3} f_0}{8 \cdot Q_s \cdot SNR} \tag{1}$$

where SNR is the signal-to-noise ratio at the RF receiver [6]. Relatively new piezoelectric materials, such as scandium alloyed AlN, have enhanced k_t^2, allowing small changes in sensor capacitance to produce relatively large shifts in resonator-sensor f_0. High Q Lamb-wave acoustic resonators (LWR) have been fabricated with these novel materials [12]–[17], making them well suited for frequency-coded passive wireless sensing. Their small size (<0.5 mm^2) in the 900 MHz ISM band makes them ideal for precision agriculture.

This work introduces a novel passive wireless soil moisture sensor node, enabled by the use of a state-of-the-art LWR in the 900 MHz ISM band. A LWR for operation in the ISM band is reported with a record FOM compared to other LWR operating at similar frequency. We demonstrate its frequency tuning capabilities by interfacing the LWR with a biodegradable capacitive soil moisture sensor [18].

II. Sensor Node Design

The sensor node is designed to be interrogated by an RF transceiver. A multi-frequency signal is sent by the base station and received by the sensor node antenna. This signal excites the resonator, which causes it to strongly vibrate at its resonant

frequency, storing RF energy in the mechanical vibrations of the resonator. Owing to the high Q of the resonator, the energy is stored long enough for the ambient reflections of the chirp to dissipate [6]. The resonator releases the electrical signal at f_0. This signal is then transmitted by the sensor antenna and its frequency is recorded at the base station [19].

Because the sensor capacitance varies with soil properties, changes in sensor capacitance alter the f_0 of the resonator. Thus, calculating the frequency of the re-radiated signal allows the acquisition of information about soil properties.

Using Keysight Advanced Design System (ADS), the sensor node equivalent circuit shown in Figure 1a, with the LWR represented as a modified Butterworth Van Dyke (mBVD) model, was built. In order to maximize sensitivity and communication range, the energy reradiated by the antenna (i.e. the energy dissipated by R_{rad} in Fig. 1a) after interrogation should be maximized. The impact of motional (R_m) and radiation (R_{rad}) resistance was investigated. With C_v, R_0 and R_s shorted, the R_{rad}/R_m ratio was varied for a resonator with $f_0 = 902\,\text{MHz}$, $Q_m = 1000$ and $k_t^2 = 9.87\%$. The power dissipated by the antenna was integrated over a period of 3τ, where $\tau = 2Q_m/(2\pi f_0)$. The antenna converts the received electromagnetic signal into a voltage (V_g) between its terminals. V_g is modeled as a voltage source applied between the leftmost node in Fig. 1a and ground. Because V_g is proportional to the square root of its radiation resistance, it was set to $\sqrt{R_{rad}}$. The results of this simulation are shown in Fig. 1b. From this plot, peak re-radiated energy occurs when $R_{rad}/R_m = 2.1$, with ranges from 1.5 to 3.2 re-radiating more than 95% of peak value. Resonator motional impedance is related to f_0, k_t^2 and Q_m in the following way:

$$R_m = \frac{1}{2\pi f_0 K^2 Q_m C_0} \tag{2}$$

where C_0 is the shunt capacitance of the resonator and $k_t^2 = \pi^2 K^2/8$. A motional impedance of $10\,\Omega$ is selected, as C_0 remains large enough to offer flexibility in LWR design, while its Q_s remains robust in the presence of small series resistances. Furthermore, $R_m = 10\,\Omega$ sets antenna radiation resistance between 15 and 32 Ω, allowing for a relatively small antenna in the 900 MHz ISM band.

A. *Lamb-Wave Resonator Design*

We designed a double-patterned (top and bottom) interdigitated electrode LWR for a motional impedance of $10\,\Omega$ in a process with 380 nm thick $Al_{0.7}Sc_{0.3}N$, and 100 nm thick AlCu electrodes. Fig. 2a illustrates how electrical potential and stress field are distributed in the LWR. The LWR exploits the enhanced d_{31} coefficient of AlScN and excites the lowest symmetric (S_0) mode. The resonant frequency is lithographically designed, as illustrated in Fig. 2a. The fabricated LWR (Fig. 2b), is composed of six electrodes with a 4.82 µm pitch and an area of 1914.7 μm^2.

We selected thick AlCu electrodes because the high conductivity of AlCu allows for low electrode resistance while its small Young's modulus (E) allows for, in LWRs,

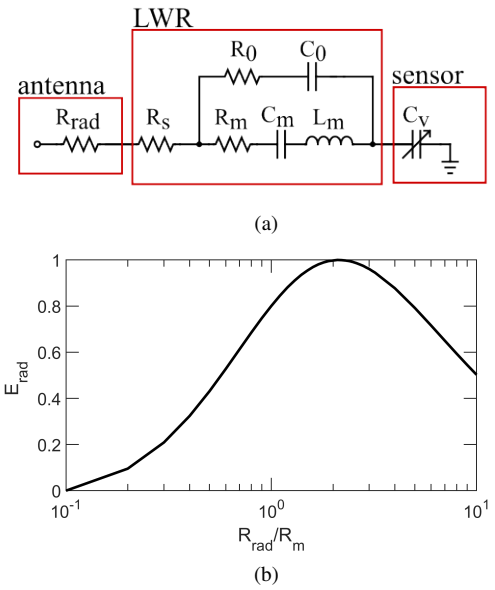

Fig. 1. (a) Sensor node equivalent circuit (b) Impact of R_{rad}/R_m on energy radiated by sensor node (E_{rad})

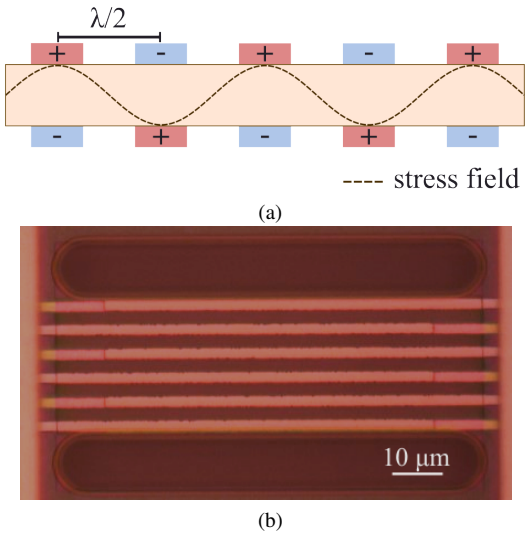

Fig. 2. (a) double-patterned LWR with stress field illustrated (b) Image of the fabricated LWR device

better k_t^2 compared to metals with larger E, such as Mo. In LWRs the electrodes are located at the points of maximum stress, unlike in bulk-acoustic wave (BAW) resonators, where they are located in the points of maximum displacement. Thus, high acoustic impedance electrodes in BAW devices allow for a more uniform and larger stress field throughout the piezoelectric material and enhance k_t^2 [20]. However, using these same high stiffness materials in LWR, where the electrodes are located at the locations of maximum stress, reduces the stress in the piezoelectric material and degrades the resonator k_t^2.

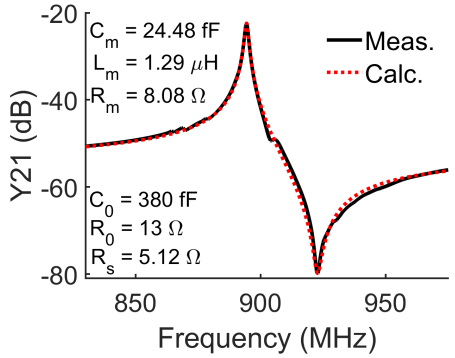

Fig. 3. Admittance of the LWR device with f_p=923 MHz and mBVD model fit and parameter values

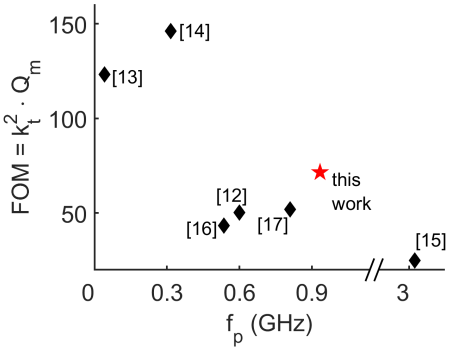

Fig. 4. Comparison of FOM with previous work on AlScN LWRs.

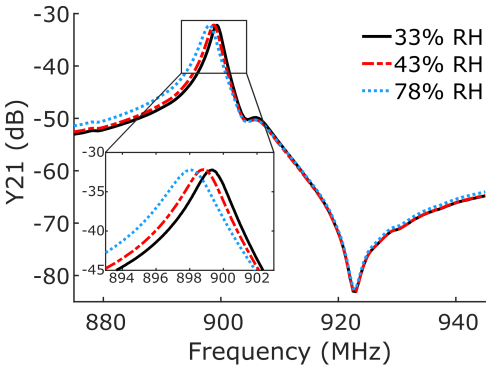

Fig. 5. Admittance of the LWR-sensor node for 3 different RH, the f_0 of the tank varies with RH

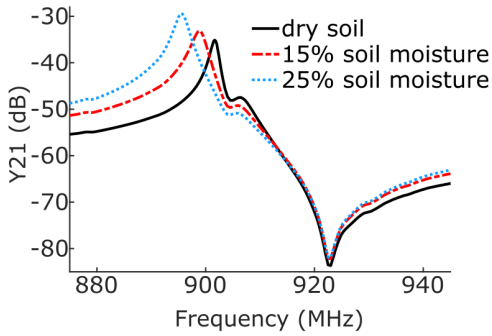

Fig. 6. Admittance of the LWR-sensor node in loamy sand for 3 different moisture levels, the f_0 of the tank decreases with soil moisture

III. Results

The LWR was fabricated in a commercial shuttle run and measured using a vector network analyzer (VNA). The VNA was calibrated using a short-open-load-through (SOLT) method on a standardized calibration set before data was collected. The device measurement was fit to a mBVD model using ADS. The measured and mBVD model of the admittance of the device are shown in Fig. 3. The device has a f_0 = 894.42 MHz, a measured Q_s of 894, and fitted k_t^2 and Q_m of 7.9% and 900 respectively. The device FOM was calculated using the mBVD model and was found to be 71.53. Fig. 4 compares this device performance with other works. At 71.53, the FOM of the device is 37.5% larger than the FOM of the LWR closest in frequency (f_0 = 801.4 MHz, FOM = 52 [17]).

The fabricated LWR was integrated with a soil moisture sensor in ADS. The sensor responds to both relative humidity (RH) in air and soil moisture. Sensor capacitance increases by 0.46 pF when RH increases from 33% to 78% [18] and by 4.9 pF when loamy sand soil moisture θ_g ($\theta_g = m_{h_2O}/m_{drysoil}$) varies from 0% to 25%. The measured sensor responses were connected in series with the measured LWR and a frequency sweep from 875-945 MHz was realized. The resulting admittance (Y21) of the LWR-sensor node is shown in Figure 5 for RH and Figure 6 for soil moisture. Because of the LWR's large k_t^2, the 45% change in RH generated a 1.4 MHz shift in f_0, while the 25% increase in soil moisture generated a 6.21 MHz shift in f_0. While the f_0 of the LWR-sensor node is shifted up from 894.42 MHz to 898-899.4 MHz and 895.5-901.71 MHz for RH and soil moisture respectively, it remains slightly below the 900 MHz ISM band. This problem is easily remedied in a future fabrication cycle by slightly decreasing the pitch of the LWR electrodes.

By inserting Q_s=894 and f_0=894.42 MHz into equation 1, and assuming a RF receiver SNR of 10, the minimum detectable frequency shift would be 64 kHz, approximately a 2.1% change in RH or less than 0.5% change in soil moisture for loamy sand. Thus, this resonator-sensor system can be used to detect small changes in soil moisture.

The maximum communication range of the system (R_{max}) can be estimated by adjusting Friis's transmission equation into the following form:

$$R_{max} = \frac{\lambda}{4\pi}\sqrt[4]{\frac{IL \cdot P_t G_t^2 G_s^2}{P_{min}}} \tag{3}$$

where λ is the wavelength of the signal, P_t is the power transmitted by the RF transceiver, G_t and G_s are transciever and sensor node antenna gain. IL is sensor insertion loss and P_{min} is the transceiver minimum detectable signal [6].

$$P_{min} = SNR \cdot kT_0 \cdot B \cdot F \tag{4}$$

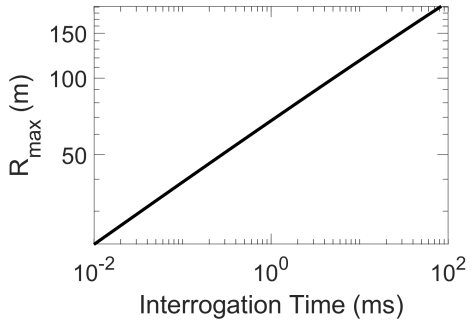

Fig. 7. Communication range as a function of sensor interrogation time

where k is Boltzmann's constant, temperature in Kelvin is T_0, and F and B are respectively transceiver noise figure and bandwidth. From ADS, for antenna $R_{rad} = 21\,\Omega$, we obtain sensor node $IL = -13\,\text{dB}$. Using values from NI B200mini software defined radio data sheet, we set $F = 8\,\text{dB}$ and $B = 56\,\text{MHz}$. Assuming $P_t = 1\,\text{W}$, $G_t = 6\,\text{dBi}$, $G_s = 0\,\text{dBi}$, a minimum required receiver SNR of 10 dB, and room temperature conditions, the maximal communication range for a single interrogation cycle is 8.5 m. However, by repeatedly pinging the sensor, we can increase interrogation time and effectively decrease the bandwidth of the transceiver [19]. From ADS simulations, sensor ringup time is approximately 400 ns, and sensor ringdown time is 650 ns. By taking this time into account for each interrogation cycle, Fig. 7 shows expected communication range as a function of total interrogation time. This boosts R_{max} significantly, with 150 m of communication range (through air) achievable with 30 ms of repeated interrogation cycles.

IV. Conclusion

This work presented the design of a passive, wireless, subsurface soil sensor node enabled by a state-of-the-art LWR for operation in the 900 MHz ISM band. A $10\,\Omega$ double patterned LWR was designed and fabricated in a commercial shuttle run. The fabricated $Al_{0.7}Sc_{0.3}N$ LWR has a FOM 37.5% larger than other AlScN LWR at similar frequency. This LWR was integrated with a biodegradable moisture sensor. The sensor's ability to tune the resonator-sensor f_0 with a sensitivity of <0.5% soil moisture ($\Delta f_0 = 65\,\text{kHz}$) was demonstrated. We illustrated how communication ranges up to 150 m at this sensitivity could be achieved.

Acknowledgment

This work is primarily supported by the IoT4Ag Engineering Research Center funded by the National Science Foundation (NSF) under NSF Award Number EEC1941529. Fabrication of the Lamb-wave resonator was supported by The Defense Advanced Research Projects Agency (DARPA) Small Business Innovation Research (SBIR) under award HR0011-21-9-0004. A.M. Zaccarin acknowledges the support of the Natural Sciences and Engineering Research Council of Canada (NSERC).

References

[1] J. Tiusanen, "Attenuation of a Soil Scout Radio Signal," *Biosystems Engineering*, vol. 90, no. 2, pp. 127–133, Feb. 2005.

[2] F. Fuschini, C. Piersanti, F. Paolazzi, and G. Falciasecca, "Analytical Approach to the Backscattering from UHF RFID Transponder," *IEEE Antennas and Wireless Propagation Letters*, vol. 7, pp. 33–35, 2008.

[3] C. Boyer and S. Roy, "— Invited Paper — Backscatter Communication and RFID: Coding, Energy, and MIMO Analysis," *IEEE Transactions on Communications*, vol. 62, no. 3, pp. 770–785, Mar. 2014.

[4] S. Kim, Y. Kawahara, A. Georgiadis, A. Collado, and M. M. Tentzeris, "Low-Cost Inkjet-Printed Fully Passive RFID Tags for Calibration-Free Capacitive/Haptic Sensor Applications," *IEEE Sensors Journal*, vol. 15, no. 6, pp. 3135–3145, Jun. 2015.

[5] S. Soodmand, A. Zhao, and G. Y. Tian, "UHF RFID system for wirelessly detection of corrosion based on resonance frequency shift in forward interrogation power," *IET Microwaves, Antennas & Propagation*, vol. 12, no. 12, pp. 1877–1884, 2018.

[6] D. Thomson, D. Card, and G. Bridges, "RF Cavity Passive Wireless Sensors With Time-Domain Gating-Based Interrogation for SHM of Civil Structures," *IEEE Sensors Journal*, vol. 9, no. 11, pp. 1430–1438, Nov. 2009.

[7] J. R. Humphries and D. C. Malocha, "Wireless SAW Strain Sensor Using Orthogonal Frequency Coding," *IEEE Sensors Journal*, vol. 15, no. 10, pp. 5527–5534, Oct. 2015.

[8] D. Malocha, J. Pavlina, D. Gallagher, N. Kozlovski, B. Fisher, N. Saldanha, and D. Puccio, "Orthogonal frequency coded SAW sensors and RFID design principles," in *2008 IEEE International Frequency Control Symposium*, May 2008, pp. 278–283.

[9] S. Kim, M. R. Adib, and K. Lee, "Development of chipless and wireless underground temperature sensor system based on magnetic antennas and SAW sensor," *Sensors and Actuators A: Physical*, vol. 297, p. 111549, Oct. 2019.

[10] W. Wang, X. Xue, S. Fan, M. Liu, Y. Liang, and M. Lu, "Development of a wireless and passive temperature-compensated SAW strain sensor," *Sensors and Actuators A: Physical*, vol. 308, p. 112015, Jun. 2020.

[11] M. Hu and F. Li Duan, "Design, fabrication and characterization of SAW devices on LiNbO3 bulk and ZnO thin film substrates," *Solid-State Electronics*, vol. 150, pp. 28–34, Dec. 2018.

[12] S. Shao, Z. Luo, and T. Wu, "High Figure-of-Merit Lamb Wave Resonators Based on Al0.7Sc0.3N Thin Film," *IEEE Electron Device Letters*, vol. 42, no. 9, pp. 1378–1381, Sep. 2021.

[13] G. Esteves, T. R. Young, Z. Tang, S. Yen, T. M. Bauer, M. D. Henry, and R. H. Olsson, "Al0.68Sc0.32N Lamb wave resonators with electromechanical coupling coefficients near 10.28%," *Applied Physics Letters*, vol. 118, no. 17, p. 171902, Apr. 2021.

[14] Z. Luo, S. Shao, K. Liu, Y. Lu, A. Mazzalai, C. Tosi, and T. Wu, "Al $_{0.7}$ Sc $_{0.3}$ N butterfly-shaped laterally vibrating resonator with a figure-of-merit ($k_t^2 \cdot Q_m$) over 146," *Applied Physics Letters*, vol. 120, no. 17, p. 173508, Apr. 2022.

[15] Z. A. Schaffer, G. Piazza, S. Mishin, and Y. Oshmyansky, "Super High Frequency Simple Process Flow Cross-Sectional Lamé Mode Resonators in 20% Scandium-Doped Aluminum Nitride," in *2020 IEEE 33rd International Conference on Micro Electro Mechanical Systems (MEMS)*, Jan. 2020, pp. 1281–1284.

[16] L. Colombo, A. Kochhar, C. Xu, G. Piazza, S. Mishin, and Y. Oshmyansky, "Investigation of 20% scandium-doped aluminum nitride films for MEMS laterally vibrating resonators," in *2017 IEEE International Ultrasonics Symposium (IUS)*, Sep. 2017, pp. 1–4.

[17] M. D. Henry, T. R. Young, E. A. Douglas, and B. A. Griffin, "Reactive sputter deposition of piezoelectric Sc0.12Al0.88N for contour mode resonators," *Journal of Vacuum Science & Technology B, Nanotechnology and Microelectronics: Materials, Processing, Measurement, and Phenomena*, vol. 36, no. 3, p. 03E104, May 2018.

[18] G. M. Iyer, A.-M. Zaccarin, R. H. Olsson III, and K. T. Turner, "Fabrication and Characterization of Cellulose-Based Materials for Biodegradable Soil Moisture Sensors," in *2022 IEEE Sensors*, 2022.

[19] W.-E. Bulst, G. Fischerauer, and L. Reindl, "State of the art in wireless sensing with surface acoustic waves," *IECON'98. Proceedings of the 24th Annual Conference of the IEEE Industrial Electronics Society*, vol. 4, pp. 2391–2396, 1998.

[20] G. G. Fattinger, "BAW resonator design considerations - An overview," in *2008 IEEE International Frequency Control Symposium*, May 2008, pp. 762–767.